

Nonlinear Quantum Optimization Algorithms via Efficient Ising Model Encodings

Taylor L. Patti,^{1,2,*} Jean Kossaifi,² Anima Anandkumar,^{3,2} and Susanne F. Yelin¹

¹*Department of Physics, Harvard University, Cambridge, Massachusetts 02138, USA*

²*NVIDIA, Santa Clara, California 95051, USA*

³*Department of Computing + Mathematical Sciences (CMS), California Institute of Technology (Caltech), Pasadena, CA 91125 USA*

Despite extensive research efforts, few quantum algorithms for classical optimization demonstrate realizable advantage. The utility of many quantum algorithms is limited by high requisite circuit depth and nonconvex optimization landscapes. We tackle these challenges to quantum advantage with two new variational quantum algorithms, which utilize multi-basis graph encodings and nonlinear activation functions to outperform existing methods with shallow quantum circuits. Additionally, both algorithms provide a polynomial reduction in measurement complexity and either a factor of two speedup *or* a factor of two reduction in quantum resources. Typically, the classical simulation of such algorithms with many qubits is impossible due to the exponential scaling of traditional quantum formalism and the limitations of tensor networks. Nonetheless, the shallow circuits and moderate entanglement of our algorithms, combined with efficient tensor method-based simulation, enable us to successfully optimize the MaxCut of high-connectivity graphs with up to 512 nodes (qubits) on a single GPU.

INTRODUCTION

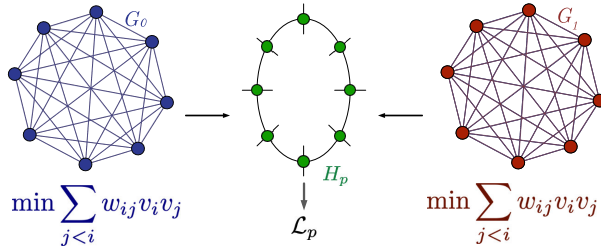
NP-hard optimization problems, such as Traveling Salesman and MaxCut, are central to a wide array of fields, such as logistics, engineering, and network design [1]. Despite the classical nature of these problems, there is immense interest in identifying variational quantum algorithms (VQAs) which solve them faster or more precisely than any classical method, a concept known as quantum advantage [2–5]. One common approach is the variational quantum eigensolver (VQE), where parameterized quantum circuits are optimized through gradient descent in order to find the ground state of a problem-encoded Hamiltonian [6–8]. The quantum approximate optimization algorithm (QAOA) is a related protocol in which parameterized rotations about both an initial and a problem encoded Hamiltonian are alternated in order to find a solution encoded ground state [9–13]. Novel VQA encoding strategies have also been considered in [14–16]. While the approximation ratios of VQE and QAOA can surpass those of polynomial complexity classical algorithms (e.g., Goemans-Williamson [17]) [18, 19], they require between polynomially and exponentially many gates in the number of qubits n . Such circuit depths can limit the algorithms’ potential to demonstrate quantum advantage, rendering them not only computationally inefficient, but also highly susceptible to quantum noise [10, 11, 20] and barren plateaus [21–26]. To combat these difficulties, alternative VQAs which demonstrate improved optimization are attracting greater interest [27].

The traditional formalism of quantum mechanics scales exponentially in n , making simulation of large quantum networks a central challenge to the development of optimization algorithms. This is due to the use of standard tensors for states (1D vectors) and operators

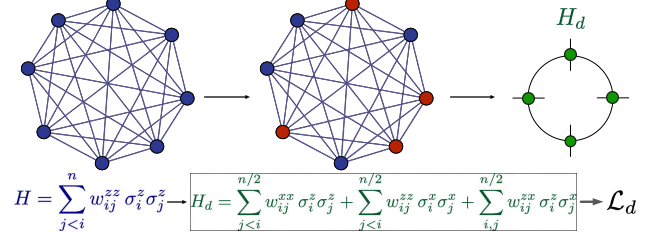
(2D matrices), which scale as 2^n and 2^{2n} , respectively. These intractable dimensions for quantum network simulation can be remediated by employing a decomposed tensor formalism [28]. While many varieties of decomposed tensors exist, tensor train (TT) has proven particularly popular in the quantum sciences due to its modularity and rank structure, which have close parallels to quantum entanglement. In the TT formalism, states $|\psi\rangle$ are represented by matrix product states (MPS) and quantum operators by matrix product operators (MPOs) [29–31]. However, TT formalism is often unsuitable for high-depth and connectivity regimes, which are most commonly used in quantum optimization, as TT tensors quickly become prohibitively large (high-rank/bond-dimension) when simulating deep or complicated circuits [32]. Moreover, they are limited to only nearest-neighbor interactions. Due in part to these limitations, no simulation of more than ~ 100 qubits [33] has demonstrated successful quantum optimization rivaling that of classical methods for non-local graph instances, with other large-scale implementations focusing on more restrictive problems. For instance, QAOA MaxCut optimization with up to 210 qubits has been achieved for highly-local 3-regular graphs [34]. It has also been implemented with several thousand qubits when exploring only local features of global graphs, a method which did not yield high average performance [35]. Moreover, large-scale MaxCut implementations using VQE have not been explored.

Our approach - This manuscript introduces two novel algorithms which can outperform traditional VQAs while requiring fewer quantum resources and lower computational complexity. In particular:

- We devise two new methods of MaxCut graph encoding, Nonlinear Parallel VQA (NP-VQA) and Nonlinear Dense VQA (ND-VQA), which, compared to traditional VQAs, which introduce additional constraints,



(a) Schematic of Nonlinear Parallel VQA (NP-VQA). Two distinct graphs, G_0 and G_1 , are mapped to the classical Ising model, save that G_1 utilizes the x , rather than the z , basis. This encoding is similar to that of the Heisenberg Hamiltonian (Eq. 6), save that the x and z -bases are addressed in separate, single-qubit Pauli strings. In addition to containing two optimization problems, the resulting parallel loss function, $\mathcal{L} = \mathcal{L}_p$ (Eq. 7), has local minima at bistable points in the (x, z) solution space and is generated by using a nonlinear activation function on the single-qubit components.



(b) Schematic of Nonlinear Dense VQA (ND-VQA). $n/2$ nodes of an n -qubit Ising model are reassigned from σ^z to σ^x operators in a manner similar to the ZX Hamiltonian, save that separate circuit preparations and measurements of single-qubit Pauli strings enable the x and z -axes of a single-qubit to represent independent vertices. When this mapping is combined with single-qubit measurements and nonlinear activation functions (similar to those of NP-VQA), only $n/2$ physical qubits are required to encode n logical qubits. The dense loss function, $\mathcal{L} = \mathcal{L}_d$ (Eq. 15), has local minima at bistable points in the (x, z) solution space.

FIG. 1

or regularization, into the optimization problem that are *beneficial* to the algorithm's performance, reducing its susceptibility to local minima in the training landscape. Moreover, these algorithms reduce runtime and hardware overhead.

- We demonstrate that NP-VQA and ND-VQA are capable of solving global optimization problems even with exceptionally shallow quantum circuits. Furthermore, we highlight that sampling multiple initializations of NP-VQA and ND-VQA on shallow circuits (with depth L approximately logarithmic in n) can efficiently address MaxCut problems [36] on quantum hardware.
- NP-VQA and ND-VQA double the time-efficiency of quantum MaxCut optimizations, *or* halve the required quantum resources, respectively. We accomplish this by encoding the classical Ising model into *both* the z and x -bases of our quantum cost function. The Heisenberg uncertainty principle is not violated by including Pauli strings along two orthogonal bases because, like other VQA protocols, NP-VQA and ND-VQA use repeated circuit preparations and measurements for each Pauli string of the loss function.
- To implement both the performance advantages of our novel algorithms and the efficiency of TT network representations, we develop TensorLy-Quantum [37], a new software package for simulating efficient quantum circuits with decomposed tensors on CPU and GPU. TensorLy-Quantum is based on the TensorLy software family [38].

- Using TensorLy-Quantum, we simulate a MaxCut problem requiring 512 logical qubits on a single NVIDIA A100 GPU and exhibit superior performance to that of comparable VQE implementations. This sets a new record for the large-scale simulation of a successful, global quantum optimization algorithm.

By introducing new algorithms which improve optimization performance, require fewer quantum resources, and operate on shallower, more error-resistant circuits, this manuscript offers tools that may narrow the gap between traditional implementations and quantum advantage.

MaxCut Optimization Problems

MaxCut is a partitioning problem on undirected graphs $G = (V, E)$, where V are the set of vertices (blue orbs in Fig. 2, left) connected by edges E (black lines connecting orbs) [36]. The objective is to optimally assign all vertices $v_i, v_j \in \{-1, 1\}$, so as to maximize the edge weights $w_{ij} \in E$, where any such assignment is referred to as a "cut". In this work, we will consider a generalized form of the problem known as *weighted* MaxCut, in which w_{ij} can take arbitrary real values.

Two formulations of MaxCut exist: the NP-complete decision problem and the NP-hard optimization problem [39]. The former seeks to determine if a cut of size c or greater exists for a given graph G , whereas the latter attempts to identify the largest cut of G possible. We here focus on the more general optimization problem formula-

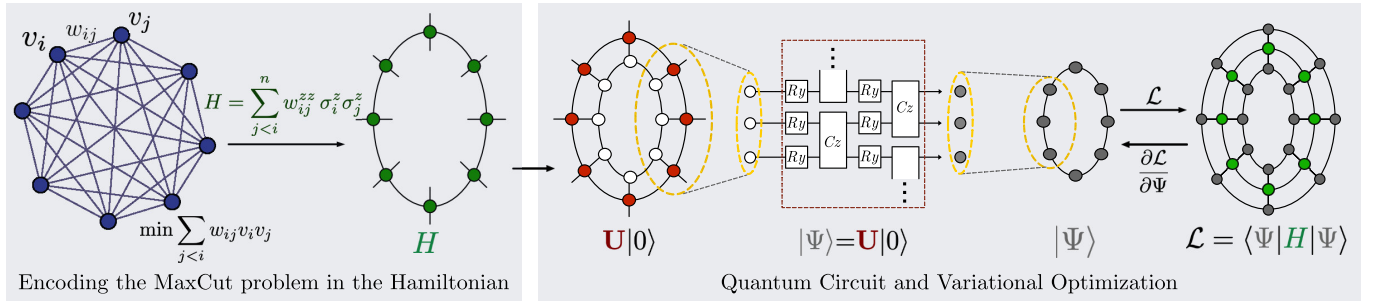


FIG. 2: Overview of traditional VQE using TT decompositions with periodic boundary conditions (tensor rings). (Left) A graph G with vertices v_i, v_j and weights w_{ij} is mapped into a Hamiltonian H in MPO form. The MPS ground state $|\psi_g\rangle$ of H encodes the solution to $\mathbf{MaxCut}(G)$. (Right) To find $\mathbf{MaxCut}(G)$ variationally, the null input state $|\mathbf{0}\rangle$ (an MPS) is evolved under a parameterized quantum circuit U (an MPO), producing an output state $|\Psi\rangle$. U encodes a circuit of depth L (here $L = 4$, red box) in this manuscript’s layer (block) pattern: one layer (block) of single-qubit y -axis rotations R_y followed by a layer of control-Z gates which alternate between even and odd qubits. The energy expectation value $\mathcal{L} = E$ is minimized via gradient descent. The global minimum of \mathcal{L} corresponds to $|\Psi\rangle = |\psi_g\rangle$.

tion, the ground truth of which we denote $\mathbf{MaxCut}(G)$. It is common practice to express this optimization in its binary quadratic form [36]

$$\text{maximize} \quad \frac{1}{2} \sum_{j < i}^n w_{ij} (1 - v_i v_j). \quad (1)$$

VQE Framework and Tensor Train Formalism

To complete MaxCut on a quantum computer, it is convenient to minimize the equivalent summation, $\sum_{j < i} w_{ij} v_i v_j$. The problem is then reduced to finding the wavefunction $|\psi\rangle$ which minimizes the energy expectation value $E = \langle \psi | H | \psi \rangle$ of the classical Ising Model Hamiltonian

$$H = \sum_{j < i}^n w_{ij}^{zz} \sigma_i^z \sigma_j^z. \quad (2)$$

H is obtained by substituting vertices v_i for the Pauli-Z spin operators σ_i^z , as depicted in Fig. 2, and $w_{ij}^{zz} = w_{ij}$ is a relabeling to specify the zz -spin interactions. As H contains only terms in the z -basis, its eigenvectors are classical (zero-entanglement product states) $|\psi_i\rangle = \bigotimes_n |n\rangle$, where $|n\rangle \in \{|0\rangle, |1\rangle\}$. We here denote the lowest eigenvalue or “ground state” solution as $|\psi_g\rangle$, the qubits of which form a bijection with the optimal v_i of $\mathbf{MaxCut}(G)$.

Fig. 2 (right) depicts the VQE framework [6–8]. Eq. 1 is optimized by defining the loss function $\mathcal{L} = E$ and varying the parameters $\hat{\theta}$ of a quantum circuit with unitary $U(\hat{\theta})$, which acts on the input quantum state (Fig. 2, right). Without loss of generality, we define the input state as the n -qubit zero state $|\mathbf{0}\rangle = \bigotimes_n |0\rangle$, such that

$$|\psi\rangle = U(\hat{\theta})|\mathbf{0}\rangle. \quad (3)$$

We can decompose this unitary matrix as Λ subunitaries $U(\hat{\theta}) = \prod_k^{\Lambda} U_k(\hat{\theta}_k)$, where $\hat{\theta}_k$ is the corresponding subset of $\hat{\theta}$ and $U_k(\hat{\theta}_k) = \prod_{j=1}^n \exp(-i\hat{\theta}_j W_j) M_k$ for generic Hermitian operators W_j and unitary matrices M_k . Thus, the gradient $g_l(\hat{O}) = \frac{\partial \langle \hat{O} \rangle}{\partial \theta_l}$ of operator \hat{O} with respect to any parameter $\theta_l \in \hat{\theta}$ is

$$g_l(\hat{O}) = i \langle \mathbf{0} | U_R^\dagger \left[W_l, U_L^\dagger \hat{O} U_L \right] U_R | \mathbf{0} \rangle, \quad (4)$$

where U_L and U_R are the compositions of unitaries U_k with $k \geq l$ and $k < l$, respectively. Rather than using deep circuits with extensive connectivity, we instead focus on 1D TT circuits of n qubits. In particular, we opt for tensor rings, which have periodic boundary conditions such that qubit $n - 1$ is connected to qubit 0. Such local connectivity makes the circuit amenable to both near-term quantum hardware [10, 12] and simulation via decomposed tensors. We accomplish this simulation with TensorLy-Quantum [37]. A nascent and expanding software package, TensorLy-Quantum strives to leverage the structure of decomposed tensors in order to simulate quantum machine learning in the most efficient, non-approximate manner possible. When judiciously constructed, TT simulations can yield a low-rank quantum formalism that permits enormous compression of state and operator spaces. Although in the quantum sciences TT methods are most frequently associated with state approximations and truncations, like the density matrix renormalization group [40], we here advocate for their use in exact quantum simulation. Similarly, due to their local connectivity, TT decompositions in quantum

computing have traditionally been employed for local optimization problems, such as 3-regular MaxCut [41], however we here emphasize their utility for global optimization tasks.

To analyze VQE with TT formalism, the MPO $H^{\{\beta, \gamma\}}$ is generated from Eq. 2. The energy $\mathcal{L} = E$ is then calculated with a single large contraction (Fig. 2, right)

$$E = \sum_{\{\beta, \gamma, \delta, \epsilon\}} \Psi^{\{\beta\}} U^{\{\beta, \gamma\}} H^{\{\gamma, \delta\}} U^{\{\delta, \epsilon\}} \Psi^{\{\epsilon\}}, \quad (5)$$

where

$$\Psi^{\{\beta\}} = \Psi^{\beta_0, \dots, \beta_{m-1}} = \sum_{\{\alpha\}} \psi_{\alpha_0 \alpha_1}^{\beta_0}, \dots, \psi_{\alpha_{m-1} \alpha_0}^{\beta_{m-1}}$$

is an n -qubit MPS of m cores and

$$U^{\{\beta, \gamma\}} = U^{\beta_0, \gamma_0, \dots, \beta_{m-1}, \gamma_{m-1}} = \sum_{\{\alpha\}} u_{\alpha_0, \alpha_1}^{\beta_0, \gamma_0}, \dots, u_{\alpha_{m-1}, \alpha_0}^{\beta_{m-1}, \gamma_{m-1}}$$

is the corresponding MPO unitary.

As we work in the absence of quantum noise, states $|\psi\rangle$ display time-reversal symmetry and can be fully expressed with real numbers [42]. We thus restrict our rotations to those of the Pauli-Y generator σ^y and implement a simple, repeating subunitary pattern of two layers, also known as blocks. The pattern is illustrated in Fig. 2 (right): a row of parameterized single-qubit rotations $R_y(\theta)$ ($W = \sigma^y$) is followed by a row of control-z (CZ) gates, with the latter alternating control between even and odd qubits. As each single qubit rotation is a 2×2 dense matrix and each two-qubit control-z gate is a rank-2 MPO of two, eight-element cores, the memory requirements of the circuit representation scale only linearly in both n and L , an exponential reduction in resources compared to circuits described in traditional quantum formalism. Likewise, TT decomposition of the input state $|\mathbf{0}\rangle$ requires exponentially fewer terms, as it is represented by a rank- $\prod_{i=0}^n 1$ MPS with just n , two-element cores.

RESULTS

Parallel VQA (NP-VQA)

Our NP-VQA method uses a loss function which is inspired by the long-range, quantum Heisenberg model for x and z -basis spin interaction

$$H_p = \sum_{j < i}^n w_{ij}^{zz} \sigma_i^z \sigma_j^z + \sum_{j < i}^n w_{ij}^{xx} \sigma_i^x \sigma_j^x, \quad (6)$$

but which encodes separate graphs into the z and x -bases and utilizes single-qubit measurements and non-linear activation functions. For simplicity, we have chosen to neglect both external fields and y -basis interactions, although we note that the addition of these terms could be used to both improve the algorithm's performance, as well as to simultaneously optimize three (rather than two) MaxCut instances. NP-VQA is depicted in Fig. 1a. Two distinct graphs, G_0 and G_1 , are mapped to the Ising model Hamiltonian in Eq. 6, save that the weights of G_1 are denoted w_{ij}^{xx} and that its vertices are parametrized with σ^x , rather than σ^z , operators. The objective is to simultaneously solve **MaxCut**(G_0) and **MaxCut**(G_1). In order to optimize these independent graphs in parallel, we must make several alterations to standard VQE. To begin, $\langle H_p \rangle$ is thus an unsuitable loss function, as its ground state's z and x -basis spin components are mutually dependent and generally encode neither **MaxCut**(G_0) nor **MaxCut**(G_1). We instead focus on the products of single-qubit measurements $\langle \sigma_i^x \rangle$ and $\langle \sigma_i^z \rangle$ such that cuts for the two graphs can be independently optimized. This yields the NP-VQA loss function

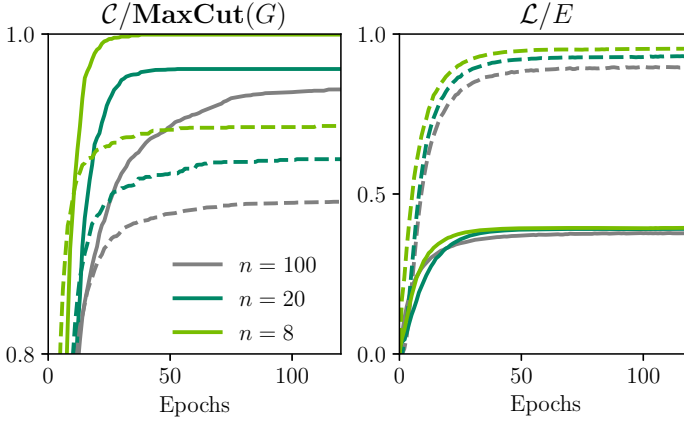
$$\mathcal{L}_p = \sum_{j < i}^n w_{ij}^{zz} \tanh(\langle \sigma_i^z \rangle) \tanh(\langle \sigma_j^z \rangle) + \sum_{j < i}^n w_{ij}^{xx} \tanh(\langle \sigma_i^x \rangle) \tanh(\langle \sigma_j^x \rangle), \quad (7)$$

where $\tanh(x)$ is trivially implemented on the classical computer controlling gradient descent. This non-linear activation function disincentives the extremization of one basis at the expense of another, which can occur because the cuts of G_0 and G_1 cannot be linearly encoded by a single quantum state due to the normalization condition of the Bloch sphere of each qubit i

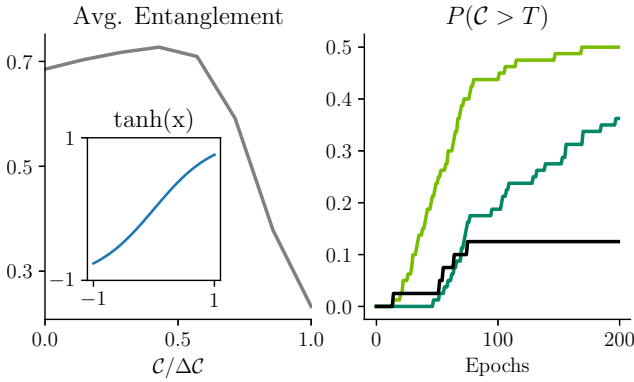
$$\langle \sigma_i^z \rangle^2 + \langle \sigma_i^x \rangle^2 \leq 1, \quad (8)$$

where equality holds for real-valued pure states. As the gradient of $\tanh(x)$ reduces near the ± 1 poles (inset Fig. 3b), full optimization of one axis at the expense of the other is discouraged and optimal cuts for both graphs can be deduced despite the normalization condition of Eq. 8. Furthermore, \mathcal{L}_p may only ever partially descend into local minima and is better equipped to escape their regions of attraction. In this manner, NP-VQA (as well as ND-VQA, detailed below) is a dual-axis quantum analog to linear programming relaxations [43].

As \mathcal{L}_p is calculated from single-qubit measurements, it can be considered a form of measurement-based quantum computation (MBQC) [44–46]. Moreover, as the number of possible single-qubit measurements scales linearly with circuit width, \mathcal{L}_p represents a polynomial reduction in the number of observables required to solve



(a) Average $\text{MaxCut}(G)$ convergence (left) and raw loss function \mathcal{L} (right) for both NP-VQA ($\mathcal{L} = \mathcal{L}_p$, solid lines) and traditional VQE ($\mathcal{L} = E$, dashed). NP-VQA improves calculated MaxCut convergence \mathcal{C} although its ability to satisfy \mathcal{L} is limited by the normalization condition of Eq. 8.



(b) (Left) Average entanglement entropy for two-qubit subpartitions (maximum value per qubit is 1) vs fraction of calculated MaxCut convergence for nonlinear loss functions. While disentanglement is not directly enforced by nonlinear loss functions and superposition is required (inset: $\tanh(x)$ loss function does not saturate ± 1 bound on domain of $\langle \sigma^\zeta \rangle$, $\zeta = z, x$), product state formation still occurs as maximizing $\langle \sigma_i^z \rangle^2 + \langle \sigma_i^x \rangle^2$ minimizes \mathcal{L}_p . (Right) The probability that a single run will converge to an optimal cut for $n = 100$, using NP-VQA with $L = 7$ (light green), $L = 1$ (dark green), and VQE with $L = 7$ (black). While the $L = 1$ case is entanglement-free, it benefits from the multi-axis superposition constraint of NP-VQA.

FIG. 3

complete graphs from $\sim n^2$ (specifically $n(n-1)/2$ two-operator Pauli strings) to $\sim 2n$ (two single-qubit measurements per qubit), lowering the measurement complexity and runtime of the algorithm on real quantum hardware [47, 48]. Numerically, \mathcal{L}_p is more compact for

large or dense graphs, where the MPO H can quickly become cumbersome. However, for the single-qubit measurements required for \mathcal{L}_p , contraction with a simple, single-qubit operator needs to occur $2n$ times. In order to efficiently compute $2n$ single-qubit measurements on large, exact tensor networks without either reconstructing an exponentially large (2^n) space or contracting over the full network $\sim n$ times, we use an efficient partial trace-based contraction scheme in which we construct k distinct reduced density matrix operators

$$\rho_k = \sum_{\{\beta, \gamma, \delta \notin K\}} \Psi^{\{\beta\}} U^{\{\beta, \gamma\}} U^{\{\gamma, \delta\}} \Psi^{\{\delta\}}, \quad (9)$$

where K is the k th set of kept indices. K should be sufficiently small so that the $2^{|K|}$ elements of ρ_k remain numerically tractable. For each ρ_k , $|K|$ smaller partial traces can be done to isolate single-qubit density matrices ρ_q , with which we take the single-qubit expectation values of Eq. 7

$$\langle \sigma_q^\zeta \rangle = \text{Tr} [\sigma_q^\zeta \rho_q], \quad (10)$$

where $\zeta = z, x$.

Not only does NP-VQA enable us to solve for the MaxCut of multiple graphs in parallel, the additional constraints increase the average performance (quotient of average cut over ground truth MaxCut) by only permitting convergence to local minima which are *bistable* points for both the z and x -axes, rather than the monostable condition of traditional VQE. Convergence to a local minima with bistability requires the concurrence of a zero gradient for both independently parametrized axes at a single, non-optimal point in parameter space. As \mathcal{L}_p is best extremized by larger $\langle \sigma^\zeta \rangle$, the circuit will tend towards satisfying the equality in Eq. 8. As this corresponds to entanglement-free qubits, there is a systematic disentanglement of the circuit into product states (Fig. 3b). To understand this process, note that for the general wavefunction

$$|\phi\rangle = \alpha|0_i0_r\rangle + \beta|0_i1_r\rangle + \gamma|1_i0_r\rangle + \delta|1_i1_r\rangle$$

describing any two qubits i and r , minimization of the loss function leads to

$$\langle \sigma_i^z \rangle^2 + \langle \sigma_i^x \rangle^2 = [(\beta + \gamma)^2 + (\alpha - \delta)^2] [(\beta - \gamma)^2 + (\alpha + \delta)^2], \quad (11)$$

which is maximized when the concurrence (entanglement [49, 50]) is minimized and vice versa. Once disentanglement nears completion, the equality in Eq. 8 begins to hold and for any θ_t and qubit i , such that

$$\langle \sigma_i^z \rangle g_t(\sigma_i^z) = -\langle \sigma_i^x \rangle g_t(\sigma_i^x), \quad (12)$$

where g_t are the gradients as given by Eq. 4. As $\langle \sigma_q^z \rangle = 0$ is unfavorable for the optimization of \mathcal{L}_p , both axes of each qubit i must be bistable with respect to each angle θ_t in order for update of that parameter to halt. In this manner, NP-VQA is a sort of quantum analog to alternating minimization in classical algorithms [51], but which uses both quantum superposition and classical nonlinearity to minimize two cost functions simultaneously, rather than one sequentially. Alternating minimization has also proven useful in QAOA protocols [15, 52–54].

As minimizing Eq. 7 cannot yield classical solutions to Eq. 1, we define a rounding scheme for the classification and scoring \mathcal{C} of $\text{MaxCut}(G)$ estimates

$$\begin{aligned} \mathcal{C}_p(\hat{\theta}; G) = & \sum_{j < i}^n \frac{w_{ij}^{zz}}{2} [1 - R(\langle \sigma_i^z \rangle)R(\langle \sigma_j^z \rangle)] \\ & + \sum_{j < i}^n \frac{w_{ij}^{xx}}{2} [1 - R(\langle \sigma_i^x \rangle)R(\langle \sigma_j^x \rangle)], \end{aligned} \quad (13)$$

where the classical function R rounds the measured expectation values to ± 1 . We note that this scoring is our true, or *computational* MaxCut estimate, as it is the MaxCut assignment which results from projecting the qubit measurements of our quantum state from the $[-0.76, 0.76]$ codomain of our linear programming relaxation ($\tanh(x)$ activation function) back into the ± 1 codomain of MaxCut nodes.

The average performance of the the NP-VQA method vs traditional VQE is displayed in Fig. 3a for registers of $n = 8, 20$, and 100 qubits. The simulations were completed using PyTorch [55] and the tensor contractions implemented with Opt-Einsum [56]. For $n = 8$ and $n = 20$, we generate exact solutions to complete (all-to-all) graphs through brute force computation, whereas the $n = 100$ graphs are the first three 0.9 density weighted MaxCut graphs (cataloged as the w09-100 instances) from the extensively studied Biq Mac library [57]. Like other recent works [22, 58], we implement simple entanglement-based pre-training prior to both the NP and ND-VQA algorithms (details in the Supplementary Information [59]). Shallow circuits of depth $L = 7$ are selected in order to adopt a protocol suitable for near-term quantum devices. While for this fixed L , both VQE and NP-VQA suffer decreasing performance with increasing n , NP-VQA consistently demonstrates a 5%-7% average performance increase across n , as seen in Fig. 3a. Finally, we again emphasize that not only is the NP-VQA algorithm more accurate than traditional VQE, it simultaneously solves $\text{MaxCut}(G)$ for *two*, rather than a single, graphs G .

While quantum optimization literature typically targets deep circuits with deterministic convergence, in what follows we reason that a probabilistic sampling of various shallow NP-VQA circuit initializations (that is, running shallower circuits multiple times) can be a more efficient alternative. As larger values of \mathcal{C} are a direct certificate of superior optimization, there should be no preference for less efficient single-shot techniques. Shallow implementations are particularly important for near-term quantum devices, which are prohibitively susceptible to noise at even moderate circuit-depth. Fig. 3b displays the probability that an optimal cut, which we define as $\mathcal{C} > T = 0.97 \times \text{MaxCut}(G)$, will be found for graphs G with $n = 100$. While studies have indicated that up to an exponential number of parameters are required to obtain nearly perfect convergence [8], a quantity that would be inconceivable for a $n = 100$ qubits, traditional VQE alone can produce optimal cuts approximately 12.5% of the time (Fig. 3b) with only seven total layers and $4n = 400$ parameters, compared to $\sim 2^{99}$ parameters for deterministic convergence. Not only would multiple repetitions r of this shallow circuit clearly be more efficient, but such probabilistic circuit sampling with NP-VQA is $4x$ more effective than with VQE for $n = 100$.

From Fig. 3b, we note that $L = 1$ circuits obtain optimal cuts with probability 0.36, tripling the convergence rate of standard VQE with 1/7th the resources. As circuits with $L = 1$ are comprised of only local rotations without control gates, the totality of the performance is due to mutual constraints on multi-basis *quantum superpositions*, and not due to quantum entanglement. Like other entanglement-free formulations [60–62], this renders the circuit efficient for classical simulation and indicates that algorithms for simulated superposition with multi-basis constraints may hold promise as “quantum inspired” classical algorithms. However, we note that quantum implementations are still of interest, because other entanglement-free relaxations are known to suffer decreased performance with increasing circuit width [8]. Furthermore, NP-VQA with even modest entanglement and circuit-depth can greatly increase the probability of optimal convergence (Fig. 4a). For depth $L = 7$, NP-VQA produces an optimal cut with 50% probability. The cumulative effects of such probabilistic sampling can lead to high-confidence convergence with markedly few repetitions r . Fig. 4a shows the probability of obtaining at least one optimal cut for $n = 100$ and $r = 5$, which nears 97% in fewer than 100 training steps for shallow NP-VQA circuits. For $r = 10$, convergence is greater than 99.9% and the $4nr = 4000$ parameters utilized for ten repetitions still pale in comparison to the exponentially many required by deep-circuit techniques.

NP-VQA also offers superior performance over traditional VQE in terms of the diversity of tenable graphs (Fig. 4a). For $r = 10$, not only does NP-VQA find optimal solutions for *all* of the complete $n = 20$ graphs tested

(compared to 90% for VQE), its parallel implementation doubles the number of MaxCut instances optimized.

Nonlinear Dense VQA (ND-VQA)

The ND-VQA paradigm also draws upon nonlinear activation functions and single-qubit measurements, but rather than *independently* encoding two graph instances into the z and x -bases, it *jointly* encodes a single n node (qubit) graph into the z and x bases of $n/2$ qubits (see Fig. 1b). We will refer to these n and $n/2$ qubit registers as the logical and physical qubits, respectively. This encoding is carried out by treating both the z and x bases of each of the $n/2$ physical qubits as a separate logical qubit, such that G can be encoded by a loss function inspired by the the ZX Hamiltonian

$$H_d = \sum_{j < i}^{n/2} w_{ij}^{zz} \sigma_i^z \sigma_j^z + \sum_{j < i}^{n/2} w_{ij}^{xx} \sigma_i^x \sigma_j^x + \sum_{i,j}^{n/2} w_{ij}^{zx} \sigma_i^z \sigma_j^x, \quad (14)$$

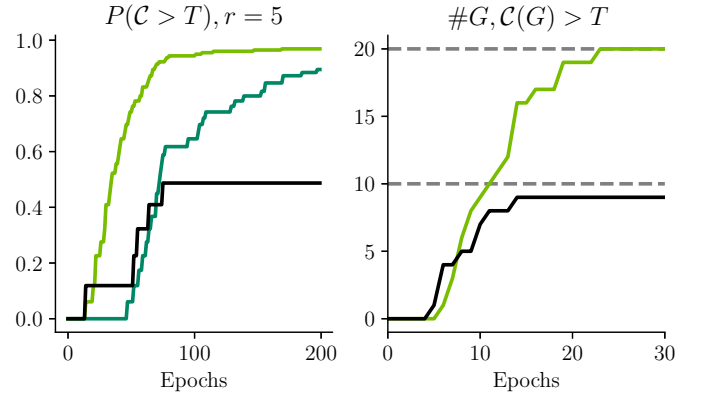
and optimized by the corresponding nonlinear loss function and rounded MaxCut estimation

$$\begin{aligned} \mathcal{L}_d = & \sum_{j < i}^{n/2} w_{ij}^{zz} \tanh(\langle \sigma_i^z \rangle) \tanh(\langle \sigma_j^z \rangle) \\ & + \sum_{j < i}^{n/2} w_{ij}^{xx} \tanh(\langle \sigma_i^x \rangle) \tanh(\langle \sigma_j^x \rangle) \\ & + \sum_{i,j}^{n/2} w_{ij}^{zx} \tanh(\langle \sigma_i^z \rangle) \tanh(\langle \sigma_j^x \rangle), \end{aligned} \quad (15)$$

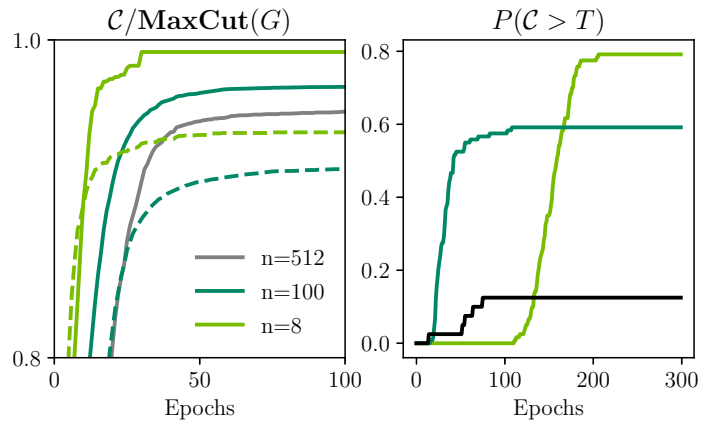
$$\begin{aligned} \mathcal{C}_d(\hat{\theta}; G) = & \sum_{j < i}^{n/2} \frac{w_{ij}^{zz}}{2} [1 - R(\langle \sigma_i^z \rangle)R(\langle \sigma_j^z \rangle)] + \\ & \sum_{j < i}^{n/2} \frac{w_{ij}^{xx}}{2} [1 - R(\langle \sigma_i^x \rangle)R(\langle \sigma_j^x \rangle)] + \\ & \sum_{i,j}^{n/2} \frac{w_{ij}^{zx}}{2} [1 - R(\langle \sigma_i^z \rangle)R(\langle \sigma_j^x \rangle)]. \end{aligned} \quad (16)$$

We again emphasize that, as Eqs. 15 and 16 are comprised of distinct Pauli strings that are independently measured on separate circuit preparations, the uncertainty principle is not violated for w_{ij}^{zx} with $j = i$.

ND-VQA doubles the number of quantum resources available, a valuable asset for a nascent field which has invested millions of dollars and spent multiple decades to achieve ~ 50 -qubit registers. Furthermore, like that of its parallel counterpart, the dual-basis constraint of ND-VQA improves MaxCut optimization. Fig. 4b illustrates



(a) (Left) The probability that at least one of $r = 5$ runs will produce an optimal cut for $n = 100$, with $L = 7$ (light green), $L = 1$ (dark green), and VQE with $L = 7$ (black). For the shallow NP-VQA $L = 7$ circuit, five repetitions produces nearly deterministic results with few epochs. (Right) Number of $n = 20$ graphs with optimal cuts for $r = 10$. NP-VQA not only successfully optimizes all (vs 90%) of G , it can solve twice as many graphs in the same number of epochs due to its parallel nature.



(b) Average $\text{MaxCut}(G)$ convergence (left) for both ND-VQA (solid lines) and traditional VQE (dashed) for $L = 7$ ($n = 8, 100$) and $L = 13$ ($n = 512$) logical qubits.

We note the dramatically increased performance for $n = 8, 100$ with ND-VQA over VQE and comment that, while VQE with $n = 512$ was prohibitively memory inefficient, ND-VQA with $n = 512$ outperforms VQE with $n = 8$, a system 1/64th of its size and still converges to optimal cuts $\sim 13\%$ of the time. Furthermore, improved optimization of the $n = 512$ would be readily attained with deeper circuits. (right) ND-VQA for $n = 100$ with $L = 13$ (light green), $L = 7$ (dark green), and VQE with $L = 7$ (black). Increasing depth from 7 to 13, while still extremely shallow for $n = 100$, greatly improves performance.

FIG. 4

the average performance of both ND-VQA and VQE circuits for $n = 8, 100$ and the ND-VQA circuit alone for the pm3-8-50 ($n = 512$) instance of the DIMACS library [63]. The pm3-8-50 ($n = 512$) with traditional VQE was too memory inefficient for evaluation on a single A100 GPU. Like its dense counterpart, ND-VQA demonstrates marked improvement over VQE in both average MaxCut convergence and probabilistic sampling.

Although our current contraction algorithm yields a maximum circuit depth of $L = 13$ for logical $n = 512$ on a single GPU, increased circuit-depth improves performance (Fig. 4b). The simulation of such deeper circuits could be provided by tensor contraction backends with improved memory management, such as the cuTensor library. Despite circuit-depth L only increasing sublogarithmically in n , ND-VQA with $n = 512$ displayed strong performance, achieving average cut of $\sim 96\%$ of the ground truth (Fig. 4b, left) and a highest accuracy upwards of 98% from thirty total runs. This exceeds not only the performance guarantees of polynomial algorithms, but also the average performance of notable specialty algorithms on this specific instance under similar specifications [64]. Moreover, ND-VQA obtains optimal cuts upwards of 13% of the time (Fig. 4b, right). While computational benchmarking has been demonstrated for thousands of qubits, to our knowledge, ND-VQA with $n = 512$ is the largest simulation of successful global quantum optimization algorithms yet conducted.

DISCUSSION

In this manuscript, we introduced the novel NP-VQA and ND-VQA algorithms. With shallow circuit-depths, their performance on the examined graphs exceed that of traditional VQAs. Both of these algorithms provide meaningful efficiency improvements and thus lower the overhead of demonstrating quantum advantage for classical optimization problems. These improvements include up to a polynomial reduction in circuit measurements, as well as a factor of two speedup for NP-VQA, and a factor of two reduction in quantum resources for ND-VQA. In actuality, both encoding methods are part of a broader framework of multi-axis qubit encodings, which include any nonlinear renormalization of quantum observables that permits the optimization of multiple, mutually regularizing observables on a single qubit. These findings are likely to spur additional research in efficient qubit encoding or the application of our techniques to related algorithms. Since deeper circuits would be attainable with more efficient tensor contraction methods or distributed computing efforts, this work encourages further development of large-scale quantum simulation with tensor methods. Most critically, as these simulations are ultimately memory-bound, the implementation of these algorithms at-scale constitutes a strong and novel

candidate for quantum advantage.

These algorithms are powerful enough to enable large-scale simulations of effective optimization algorithms on a single, consumer-grade GPU. To our knowledge, we were able to produce the largest simulation of a quantum global optimization algorithm which rivals classical performance achieved to-date. Such a successful and large-scale implementation demonstrates that exceedingly simple and low-rank TT representations are sufficient to model diverse techniques in quantum machine learning, and to do so without truncation or approximation. Finally, through the use of large-scale global graphs, we demonstrate that the local connectivity and low entanglement capacity of both the MPS formalism and linearly connected near-term quantum devices do not preclude successful quantum optimization routines. When we expand our definition of accuracy to encompass probabilistic sampling of various circuit initializations, we find that remarkably few quantum resources can be requisite for classical optimization problems.

ACKNOWLEDGEMENTS

This work was done during T.L.P.’s internship at NVIDIA. At CalTech, A.A. is supported in part by the Bren endowed chair, and Microsoft, Google, Adobe faculty fellowships. S.F.Y. thanks the AFOSR and the NSF for funding through the CUA-PFC grant. The authors would like to thank Brucek Khailany, Johnnie Gray, Garret Chan, Andreas Hehn, and Adam Jedrych for conversations.

AUTHOR CONTRIBUTIONS

T.L.P. and J.K. contributed to all aspects of the work. A.A. contributed context on machine learning and classical algorithms. S.F.Y. contributed context on quantum information-related physics. A.A. and S.F.Y. contributed guidance on the research and manuscript.

COMPETING INTERESTS

The authors claim no competing interests.

* taylorpatti@g.harvard.edu
 [1] Li, W. *et al.* Parameterized algorithms of fundamental np-hard problems: a survey. *Human-centric Computing and Information Sciences* **10**, 29 (2020). URL <https://doi.org/10.1186/s13673-020-00226-w>.

[2] Lucas, A. Ising formulations of many np problems. *Frontiers in Physics* **2**, 5 (2014). URL <https://www.frontiersin.org/article/10.3389/fphy.2014.00005>.

[3] Wecker, D., Hastings, M. B. & Troyer, M. Progress towards practical quantum variational algorithms. *Phys. Rev. A* **92**, 042303 (2015). URL <https://link.aps.org/doi/10.1103/PhysRevA.92.042303>.

[4] McClean, J. R., Romero, J., Babbush, R. & Aspuru-Guzik, A. The theory of variational hybrid quantum-classical algorithms. *New Journal of Physics* **18**, 023023 (2016). URL <https://doi.org/10.1088%2F1367-2630%2F18%2F2%2F023023>.

[5] Cerezo, M. *et al.* Variational quantum algorithms (2020). 2012.09265.

[6] Peruzzo, A. *et al.* A variational eigenvalue solver on a photonic quantum processor. *Nature Communications* **5**, 4213 (2014). URL <https://doi.org/10.1038/ncomms5213>.

[7] Kandala, A. *et al.* Hardware-efficient Quantum Optimizer for Small Molecules and Quantum Magnets. *Nature Publishing Group* **549**, 242–246 (2017). URL <https://arxiv.org/abs/1704.05018>. 1704.05018.

[8] Lee, J., Magann, A. B., Rabitz, H. A. & Arenz, C. Towards favorable landscapes in quantum combinatorial optimization (2021). 2105.01114.

[9] Farhi, E., Goldstone, J. & Gutmann, S. A quantum approximate optimization algorithm. *arXiv* (2014). 1411.4028.

[10] Harrigan, M. P. *et al.* Quantum approximate optimization of non-planar graph problems on a planar superconducting processor. *Nature Physics* **3**, 1745 (2021). URL <https://doi.org/10.1038/s41567-020-01105-y>.

[11] Guerreschi, G. G. & Matsudaira, A. Y. Qaoa for max-cut requires hundreds of qubits for quantum speed-up. *Scientific Reports* **9**, 6903 (2019). URL <https://doi.org/10.1038/s41598-019-43176-9>.

[12] Pagano, G. *et al.* Quantum approximate optimization of the long-range ising model with a trapped-ion quantum simulator. *Proceedings of the National Academy of Sciences* **117**, 25396–25401 (2020). URL <https://www.pnas.org/content/117/41/25396>. <https://www.pnas.org/content/117/41/25396.full.pdf>.

[13] Zhou, L., Wang, S.-T., Choi, S., Pichler, H. & Lukin, M. D. Quantum approximate optimization algorithm: Performance, mechanism, and implementation on near-term devices. *Phys. Rev. X* **10**, 021067 (2020). URL <https://link.aps.org/doi/10.1103/PhysRevX.10.021067>.

[14] Kim, I. H. & Swingle, B. Robust entanglement renormalization on a noisy quantum computer (2017). 1711.07500.

[15] Wang, Z., Rubin, N. C., Dominy, J. M. & Rieffel, E. G. xy mixers: Analytical and numerical results for the quantum alternating operator ansatz. *Phys. Rev. A* **101**, 012320 (2020). URL <https://link.aps.org/doi/10.1103/PhysRevA.101.012320>.

[16] Fuchs, F. G., Kolden, H., Øie, A., Henrik, N. & Sartor, G. Efficient encoding of the weighted max k -cut on a quantum computer using qaoa. *SN Computer Science* **2**, 2661–8907 (2021). URL <https://doi.org/10.1007/s42979-020-00437-z>.

[17] Goemans, M. X. & Williamson, D. P. Improved approximation algorithms for maximum cut and satisfiability problems using semidefinite programming. *J. of the ACM* **42**, 1115 (1995).

[18] Håstad, J. Some optimal inapproximability results. *J. ACM* **48**, 798–859 (2001). URL <https://doi.org/10.1145/502090.502098>.

[19] Khot, S., Kindler, G., Mossel, E. & O'Donnell, R. Optimal inapproximability results for max-cut and other 2-variable csps? *SIAM* **37**, 319 (2005). URL <https://www.cs.cmu.edu/~odonnell/papers/maxcut.pdf>.

[20] Preskill, J. Quantum Computing in the NISQ era and beyond. *Quantum* **2**, 79 (2018). URL <https://doi.org/10.22331/q-2018-08-06-79>.

[21] McClean, J. R., Boixo, S., Smelyanskiy, V. N., Babbush, R. & Neven, H. Barren plateaus in quantum neural network training landscapes. *Nature Communications* **9**, 4812 (2018). URL <https://doi.org/10.1038/s41467-018-07090-4>.

[22] Patti, T. L., Najafi, K., Gao, X. & Yelin, S. F. Entanglement devised barren plateau mitigation (2020). 2012.12658.

[23] Marrero, C. O., Kieferová, M. & Wiebe, N. Entanglement Induced Barren Plateaus (2020). URL <https://arxiv.org/abs/2010.15968>. 2010.15968.

[24] Wiersema, R. *et al.* Exploring entanglement and optimization within the hamiltonian variational ansatz. *PRX Quantum* **1**, 020319 (2020). URL <https://link.aps.org/doi/10.1103/PRXQuantum.1.020319>.

[25] Holmes, Z., Sharma, K., Cerezo, M. & Coles, P. J. Connecting ansatz expressibility to gradient magnitudes and barren plateaus (2021). 2101.02138.

[26] Cerezo, M., Sone, A., Volkoff, T., Cincio, L. & Coles, P. J. Cost-function-dependent barren plateaus in shallow quantum neural networks (2020). URL <https://arxiv.org/abs/2001.00550>. 2001.00550.

[27] Amaro, D. *et al.* Filtering variational quantum algorithms for combinatorial optimization (2021). 2106.10055.

[28] Fishman, M., White, S. R. & Stoudenmire, E. M. The itensor software library for tensor network calculations (2020). 2007.14822.

[29] Orús, R. A practical introduction to tensor networks: Matrix product states and projected entangled pair states. *Annals of Physics* **349**, 117–158 (2014). URL <https://www.sciencedirect.com/science/article/pii/S0003491614001596>.

[30] Bridgeman, J. C. & Chubb, C. T. Hand-waving and interpretive dance: an introductory course on tensor networks. *Journal of Physics A: Mathematical and Theoretical* **50**, 223001 (2017).

[31] Huggins, W., Patil, P., Mitchell, B., Whaley, K. B. & Stoudenmire, E. M. Towards quantum machine learning with tensor networks. *Quantum Science and Technology* **4**, 024001 (2019). URL <https://doi.org/10.1088/2058-9565/aaea94>.

[32] Zhou, Y., Stoudenmire, E. M. & Waintal, X. What limits the simulation of quantum computers? *Phys. Rev. X* **10**, 041038 (2020). URL <https://link.aps.org/doi/10.1103/PhysRevX.10.041038>.

[33] Fried, E. S. *et al.* qtorch: The quantum tensor contraction handler. *PLOS ONE* **13**, 1–20 (2018). URL <https://doi.org/10.1371/journal.pone.0208510>.

[34] Lykov, D., Schutski, R., Galda, A., Vinokur, V. & Alexeev, Y. Tensor network quantum simulator with step-dependent parallelization (2020). 2012.02430.

[35] Huang, C. *et al.* Alibaba cloud quantum development platform: Applications to quantum algorithm design

(2019). 1909.02559.

[36] Commander, C. W. *Maximum cut problem, MAX-CUTMaximum Cut Problem, MAX-CUT*, 1991–1999 (Springer US, Boston, MA, 2009). URL https://doi.org/10.1007/978-0-387-74759-0_358.

[37] Patti, T. L., Kossaifi, J. & Anandkumar, A. Tensorly-quantum: Tensor-based quantum machine learning (2021). URL <https://github.com/tensorly/quantum>.

[38] Kossaifi, J., Panagakis, Y., Anandkumar, A. & Pantic, M. Tensorly: Tensor learning in python. *J. Mach. Learn. Res.* **20**, 925–930 (2019).

[39] Karp, R. M. (1972).

[40] White, S. R. Density matrix formulation for quantum renormalization groups. *Phys. Rev. Lett.* **69**, 2863–2866 (1992). URL <https://link.aps.org/doi/10.1103/PhysRevLett.69.2863>.

[41] Wurtz, J. & Love, P. Maxcut quantum approximate optimization algorithm performance guarantees for $p > 1$. *Phys. Rev. A* **103**, 042612 (2021). URL <https://link.aps.org/doi/10.1103/PhysRevA.103.042612>.

[42] Shen, H., Zhang, P., You, Y.-Z. & Zhai, H. Information scrambling in quantum neural networks. *Phys. Rev. Lett.* **124**, 200504 (2020). URL <https://link.aps.org/doi/10.1103/PhysRevLett.124.200504>.

[43] Aardal, K. & Weismantel, R. *Polyhedral combinatorics : an annotated bibliography*. Universiteit Utrecht. UU-CS, Department of Computer Science (Utrecht University, Netherlands, 1996).

[44] Raussendorf, R. & Briegel, H. J. A one-way quantum computer. *Phys. Rev. Lett.* **86**, 5188–5191 (2001). URL <https://link.aps.org/doi/10.1103/PhysRevLett.86.5188>.

[45] Raussendorf, R., Browne, D. E. & Briegel, H. J. Measurement-based quantum computation on cluster states. *Phys. Rev. A* **68**, 022312 (2003). URL <https://link.aps.org/doi/10.1103/PhysRevA.68.022312>.

[46] Ferguson, R. R. *et al.* Measurement-based variational quantum eigensolver. *Phys. Rev. Lett.* **126**, 220501 (2021). URL <https://link.aps.org/doi/10.1103/PhysRevLett.126.220501>.

[47] Verteletskyi, V., Yen, T.-C. & Izmaylov, A. F. Measurement optimization in the variational quantum eigensolver using a minimum clique cover. *J. Chem. Phys.* **152** (2020). URL <https://doi.org/10.1063/1.5141458>.

[48] Shehab, O. *et al.* Noise reduction using past causal cones in variational quantum algorithms (2019). 1906.00476.

[49] Wootters, W. K. Entanglement of formation and concurrence. *Quantum Info. Comput.* **1**, 27–44 (2001).

[50] Gao, X., Sergio, A., Chen, K., Fei, S. & Li-Jost, X. Entanglement of formation and concurrence for mixed states. *Front. Comput. Sci.-Chi* **2**, 114 (2008).

[51] Jain, P. & Kar, P. Non-convex optimization for machine learning. *Foundations and Trends® in Machine Learning* **10**, 142–363 (2017). URL <http://dx.doi.org/10.1561/2200000058>.

[52] Hadfield, S. *et al.* From the quantum approximate optimization algorithm to a quantum alternating operator ansatz. *Algorithms* **12** (2019). URL <https://www.mdpi.com/1999-4893/12/2/34>.

[53] Zhu, L. *et al.* An adaptive quantum approximate optimization algorithm for solving combinatorial problems on a quantum computer (2020). 2005.10258.

[54] Cook, J., Eidenbenz, S. & Bärtschi, A. The quantum alternating operator ansatz on maximum k-vertex cover (2020). 1910.13483.

[55] Paszke, A. *et al.* Pytorch: An imperative style, high-performance deep learning library. In Wallach, H. *et al.* (eds.) *Advances in Neural Information Processing Systems*, vol. 32 (Curran Associates, Inc., 2019). URL <https://proceedings.neurips.cc/paper/2019/file/bdbca288fee7f92f2bfa9f7012727740-Paper.pdf>.

[56] a. Smith, D. G. & Gray, J. opt_einsum - a python package for optimizing contraction order for einsum-like expressions. *Journal of Open Source Software* **3**, 753 (2018). URL <https://doi.org/10.21105/joss.00753>.

[57] Wiegele, A. Biq mac library – a collection of max-cut and quadratic 0-1 programming instances of medium size. Tech. Rep. (2007).

[58] Dborin, J., Barratt, F., Wimalaweera, V., Wright, L. & Green, A. G. Matrix product state pre-training for quantum machine learning (2021). 2106.05742.

[59] to be Inserted by Publisher, L.

[60] Wang, T. & Roychowdhury, J. Oim: Oscillator-based ising machines for solving combinatorial optimisation problems (2019). 1903.07163.

[61] Goto, H., Tatsumura, K. & Dixon, A. R. Combinatorial optimization by simulating adiabatic bifurcations in nonlinear hamiltonian systems. *Science Advances* **5** (2019). URL <https://advances.sciencemag.org/content/5/4/eaav2372>. <https://advances.sciencemag.org/content/5/4/eaav2372.full.pdf>.

[62] Crosson, E. & Harrow, A. W. Simulated quantum annealing can be exponentially faster than classical simulated annealing. *2016 IEEE 57th Annual Symposium on Foundations of Computer Science (FOCS)* (2016). URL <http://dx.doi.org/10.1109/FOCS.2016.81>.

[63] he dimacs library of mixed semidefinite-quadratic-linear programs. URL <http://dimacs.rutgers.edu/Challenges/Seventh/Instances/>.

[64] Burer, S., Monteiro, R. D. C. & Zhang, Y. Rank-two relaxation heuristics for max-cut and other binary quadratic programs. *SIAM J. Optim.* (2001).